Bi-label Propagation for Generic Multiple Object Tracking

Wenhan Luo[1], Tae-Kyun Kim[1], Björn Stenger[2], Xiaowei Zhao[1], Roberto Cipolla[3]
[1]Imperial College London, [2]Toshiba Research Europe, [3]University of Cambridge
{w.luo12,tk.kim,x.zhao}@imperial.ac.uk, bjorn@cantab.net, cipolla@eng.cam.ac.uk

Abstract

In this paper, we propose a label propagation framework to handle the multiple object tracking (MOT) problem for a generic object type (cf. pedestrian tracking). Given a target object by an initial bounding box, all objects of the same type are localized together with their identities. We treat this as a problem of propagating bi-labels, i.e. a binary class label for detection and individual object labels for tracking. To propagate the class label, we adopt clustered Multiple Task Learning (cMTL) while enforcing spatio-temporal consistency and show that this improves the performance when given limited training data. To track objects, we propagate labels from trajectories to detections based on affinity using appearance, motion, and context. Experiments on public and challenging new sequences show that the proposed method improves over the current state of the art on this task.

1. Introduction

Multiple Object Tracking (MOT) plays an important role in the computer vision literature. The problem is difficult due to frequent occlusions and appearance similarity between objects. Owing to advances in object detection (especially in pedestrian detection [9, 11]), in some cases the task can be solved efficiently using a tracking-as-detection approach. However, generalizing the task to other objects (see our data sets in Sec. 4) would require training a detector for each new object type, which is impractical.

In this paper we deal with the problem of tracking multiple objects of the same generic type given only one initial bounding box [18], and our task is to recover multiple trajectories from image observations. Treating sliding windows as points in a spatio-temporal cuboid and the initial bounding box as a single labeled point, we aim to discover and track new objects by propagating labels to similar candidates. From this perspective, our problem shares great similarity with semantic video segmentation [3] which aims to label all the pixels in a video given pixel labels in the first frame. However, these two problems have significant dif-
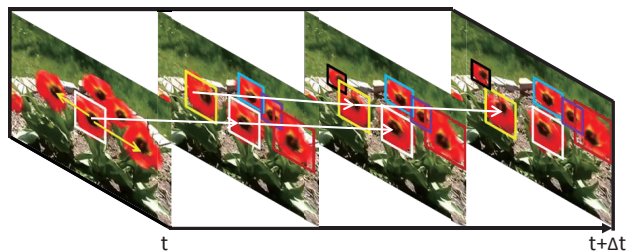

Figure 1: *The proposed framework. Yellow arrows indicate the propagation of class labels within the same frame and white arrows indicate object label propagation over time (best viewed in color).*

ferences: labels in video segmentation involve only a fixed number of pre-defined classes, whereas labels in our problem involve both binary classes (object *vs.* background) and multiple classes (specific object identities). Thus the number of classes in our problem varies as objects appear or disappear. Also, in video segmentation more than one pixel can share the same label while in our case object labels are exclusive.

We treat the labels as a combination of *binary class labels* and *object labels* (identities), and we refer to detection responses as an intermediate layer between image observations and trajectory estimations. Furthermore, we propose a sequential label propagation framework (Fig. 1) to propagate class labels and object labels in both spatial and temporal domains. This so called *bi-label propagation* framework coincides with a tracking-by-detection strategy: through spatially propagating the class labels (yellow arrows in Fig. 1), we solve the detection problem, discovering the appearance and disappearance of objects; by temporally propagating object labels (white arrows in Fig. 1), we tackle the multi-object tracking problem.

Learning a robust detector from a single training instance is challenging and standard methods tend to either overfit (*e.g.* using a kernel Support Vector Machine (SVM)) or underfit (*e.g.* using a linear SVM). To address the generalization issue, we train multiple detectors inspired by ensemble learning. Multiple detectors are inherently related to each other since they are dealing with the same type of objects.

The motivation of Multiple Task Learning (MTL) [10] is to learn multiple related tasks simultaneously rather than independently. Thus, we treat training each of the detectors as one task and adopt clustered MTL (cMTL) [32] to regularize the training process of multiple detectors. In addition, we assume that images and hence detection results do not change drastically from frame to frame. We model this spatio-temporal consistency by integrating it into the cMTL formula during the class label propagation.

Our key contributions are (1) proposing a probabilistic framework for jointly propagating class and object labels in spatial and temporal domains for generic MOT and (2) introducing cMTL for generic object detection and improving it by considering the spatio-temporal consistency.

2. Related work

MOT methods can be grouped into two categories [23]: sequential (or online) approaches, which output trajectories on the fly, and batch (or off-line) approaches, which output results after processing all frames.

Sequential approaches derive a cost function and estimate the lowest cost state based on sophisticated appearance, motion and interaction models. For example, to maintain discrimination of individual objects, Yang *et al*. [29] fuse multiple components: bags of local features, a head model, and a color model of torso regions. In [6], generic object category and instance-specific information are integrated to track multiple objects in a particle filter framework. Inspired by crowd simulation models, a dynamic model considering social motion patterns is introduced in [21]. Similarly, Yamaguchi *et al*. [27] develop an agent-based behavior model taking social and environmental factors into account to predict destinations of pedestrians. The work in [14] estimates object motion based on structured crowd patterns and learns spatio-temporal variations using a set of hidden Markov models.

Batch approaches exhibit a delay in outputting results, but they tend to be more robust as they can access all observations simultaneously. Typical batch approaches [7, 12, 15, 28] cast the problem as a data association problem, linking short-term observations such as single detection responses or tracklets into longer trajectories using methods such as the Hungarian algorithm [25], greedy bipartite matching [24], min-cost network flow [8, 26], K-Shortest Paths [4], or discrete-continuous Conditional Random Fields (CRF) [19].

Methods for generic object detection in video data require either pre-trained detectors [30] or off-line training [1]. Models are adapted to a given input video in order to improve the detection accuracy, *e.g.* by iterative boosting [1].

The closest work to ours is coupled detection and tracking [16, 26]. However, most work assumes that a detector
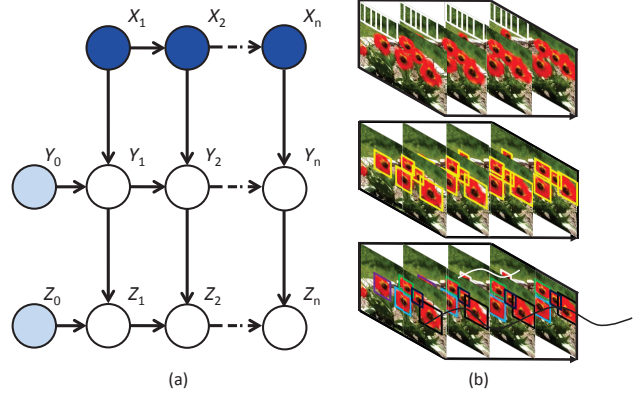

Figure 2: *(a) Our graphical model. (b) Top to bottom: sliding windows X, detection responses Y, and trajectories Z. For sake of display, we only show two trajectories (best viewed in color).*

is available that has been trained off-line. For example, [26] use a dictionary of foreground images for pedestrian detection together with background subtraction. The work in [16] employs off-line trained pedestrian and car detectors. In terms of problem setting, we follow the model-free approaches in [18, 31]. The method of Zhang and van der Maaten requires initialization with bounding boxes of all objects and in contrast to our method does not discover new similar objects [31]. Luo and Kim first train a generic object detector, and subsequently employ the detector to regularize the training of multiple trackers [18]. In contrast to this approach, we learn detection with the help of tracking, *i.e.* the spatio-temporal consistency, as well as tracking based on detection, in a joint optimization framework.

3. Bi-label Propagation

3.1. Bayesian perspective

Let X, Y and Z represent sliding windows (image observations), detection responses and trajectories, respectively. Fig. 2(a) shows our graphical model which has three layers: image observation, detection, and trajectory layer, respectively. The darkly shaded nodes are observed nodes, the transparent nodes are hidden (or latent) nodes, and the lightly shaded nodes (Y_0 and Z_0) are partly observed as we are given only a single initial bounding box in the first frame. From the image layer to the detection response layer we propagate class labels. From the detection response layer to the trajectory layer we propagate object labels. Solving our problem corresponds to maximizing $P(Z|X)$. Introducing variable Y, we obtain

$$\max_Z P(Z|X) \propto \max_{Z,Y} P(Z|X,Y)P(Y|X)$$
$$= \max_{Z,Y} \prod_t P(Z_t|X_t, Y_t, Z_{0:t-1})P(Y_t|X_t, Y_{t-1}), \quad (1)$$

where $P(Y|X)$ models class label propagation (detection) and $P(Z|X, Y)$ models object label propagation (tracking). We expand it sequentially as

$$\max_{Z_t, Y_t} P(Z_t|X_t, Y_t, Z_{0:t-1})P(Y_t|X_t, Y_{t-1}), \quad (2)$$

and solve this estimation problem by decomposition. Taking the negative logarithm of Eq. 2, we rewrite it as:

$$\min_{\mathbf{W}_t, \mathbf{\Theta}_t} \mathcal{L}_C(\mathbf{W}_t) + \mathcal{L}_O(\mathbf{\Theta}_t), \quad (3)$$

where $\mathcal{L}_C(\mathbf{W}_t)$ models class label propagation, $\mathcal{L}_O(\mathbf{\Theta}_t)$ models object label propagation and $\mathbf{W}_t, \mathbf{\Theta}_t$ are parameters representing the detector and propagation configuration at time t. To minimize the function, we

(1) fix $\mathbf{\Theta}_{t-1}$ to minimize $\mathcal{L}_C$ via $\mathbf{W}_t$;
(2) fix $\mathbf{W}_t$, minimize $\mathcal{L}_O$ via $\mathbf{\Theta}_t$;
(3) $t \leftarrow t + 1$ (go to the next frame).

3.2. Class label propagation

Let us review the Bayesian formula of class label propagation $P(Y_t|X_t, Y_{t-1})$ in Eq. 2. We want to maximize the likelihood of Y_t conditioned on observations X_t (spatial domain) and the previous estimation Y_{t-1} (temporal domain).

Our detection problem differs from the traditional detection problem as we do not have sufficient data to handle large intra-class variation. Fig. 3 illustrates the extent of intra-class variation in three test videos.

As training a single classifier leads to underfitting or overfitting, we train multiple detectors and make a decision based on all of them. Moreover, by treating training each detector as one task, we investigate the relationship among multiple detectors and adopt clustered MTL to train these detectors simultaneously, improving the generalization ability.

In the first frame, we add small perturbations to the initial bounding box (slight shift, rotation, scale changes) to augment the positive data. Sliding windows with an overlap (intersection/union) of the positive samples between 0.2 and 0.3 are negative samples. In the following frames, we collect confident instances as positive samples and augment the training data in the same way.

By randomly sampling a subset of instances from the whole training data without placement m times, we obtain m sets of training data $\mathbf{X}_{l,t,i} \in \mathbb{R}^{d \times N_{t,i}}, i = 1, ..., m$ and their labels $\mathbf{Y}_{t,i} \in \{1, -1\}^{N_{t,i}}$, where the subscript "l" means "labeled", d is the feature space dimension and $N_{t,i}$ is the number of instances. Let the multiple detectors be $\mathbf{W} = [\mathbf{w}_1, ..., \mathbf{w}_m] \in \mathbb{R}^{d \times m}$. Using the least square error the data cost term is $\sum_{i=1}^m \|\mathbf{X}_{l,t,i}^T \mathbf{w}_{t,i} - \mathbf{Y}_{t,i}\|^2$. The detectors are related as they are dealing with objects of the same type. Meanwhile, as a result of data distribution a cluster of instances are more similar to each other compared with
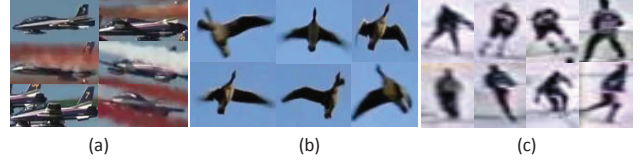

Figure 3: *Illustration of intra-class variance. Shown are cropped regions from (a) the* Airshow *sequence, (b) the* Goose *sequence and (c) the* Hockey *sequence.*

others, *e.g.* some instances exhibit a similar viewpoint while some do not. Consequently, some detectors will be closer to each other in the model parameter space. We therefore assume that the detectors form k clusters as $\mathcal{C}_j, j = 1, ..., k$, and model the coupling among all detectors following [32]:

$$\sum_{j=1}^k \sum_{v \in \mathcal{C}_j} \|\mathbf{w}_v - \bar{\mathbf{w}}_j\|^2 = tr(\mathbf{W}^T \mathbf{W}) - tr(\mathbf{F}^T \mathbf{W}^T \mathbf{W} \mathbf{F}), \quad (4)$$

where $\bar{\mathbf{w}}_j$ is the mean of the detectors within the same cluster, $tr(\bullet)$ is the trace norm, and $\mathbf{F} \in \mathbb{R}^{m \times k}$ is an orthogonal cluster indicator matrix with $\mathbf{F}_{i,j} = \frac{1}{\sqrt{n_j}}$ if $i \in \mathcal{C}_j$ and $\mathbf{F}_{i,j} = 0$ otherwise. Along with regularization of each detector $\sum_{i=1}^m \|\mathbf{w}_i\|^2 = tr(\mathbf{W}^T \mathbf{W})$, we have a regularization term $tr(\mathbf{W}((1+\eta)\mathbf{I} - \mathbf{F}\mathbf{F}^T)\mathbf{W}^T)$, where η is a weight parameter. Following the convex relaxation of cMTL [32], this regularization term is relaxed to $tr(\mathbf{W}(\eta\mathbf{I} + \mathbf{M})^{-1}\mathbf{W}^T)$, subject to $tr(\mathbf{M}) = k, \mathbf{M} \preceq \mathbf{I}, \mathbf{M} \in \mathbf{S}_+^m$, where $\mathbf{S}_+^m$ is the set of positive semi-definite (PSD) matrices and $\mathbf{M} \preceq \mathbf{I}$ means $\mathbf{I} - \mathbf{M}$ is PSD.

Traditional MOT applies a detector to every frame independently. By contrast, we find that detection responses in two subsequent frames should not change drastically. To utilize such information, we track confident instances via a weak tracker (KLT in our implementation) from frame $t-1$ to frame t, and produce a density map P_t (see an example in Fig. 4(d)) by smoothing the confidence scores with a Gaussian ($\sigma = 5$). Based on P_t, sliding windows $\mathbf{X}_{u,t} \in \mathbb{R}^{d \times N}$ (here the subscript "u" means "unlabeled") can be weakly labeled as $\mathbf{\Psi}(P_t)$ which is the summation of the density of pixels close to their centers (within a circle of radius 4). The cost term $\|\frac{1}{m}\sum_{i=1}^m \mathbf{X}_{u,t}^T \mathbf{w}_{t,i} - \mathbf{\Psi}(P_t)\|^2$ can be considered as a weakly supervised term which propagates labels in the temporal domain. Intuitively, it assists the detector to recall more instances; Fig. 4 shows this concept. Yellow boxes indicate the detection results (also positive instances), black boxes are negative instances, and white boxes are unlabeled samples. With the help of spatio-temporal consistency, some candidates have weak labels indicated by the orange boxes in frame t shown in Fig. 4(e), and the weak labels help to recover missed detections, see the dashed yellow box in frame t in Fig. 4(f) which is a missed detection caused by occlusion in Fig. 4(c). Based on the terms de-
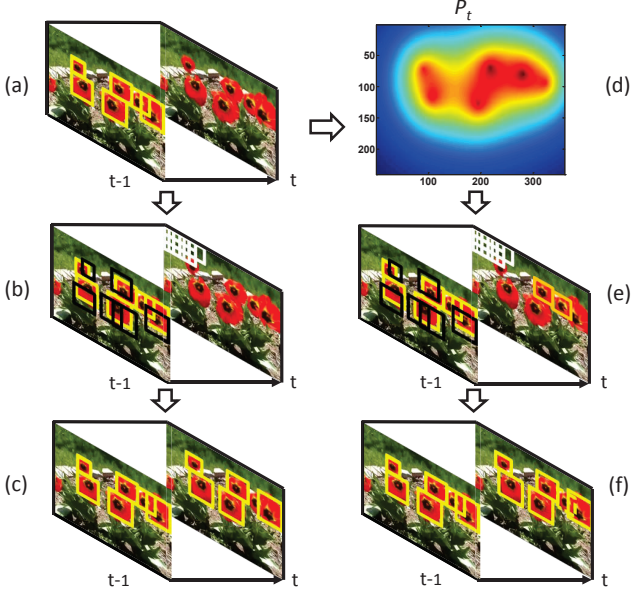
Figure 4: *Illustration of how the spatio-temporal consistency guides the detection procedure (best viewed in color).*
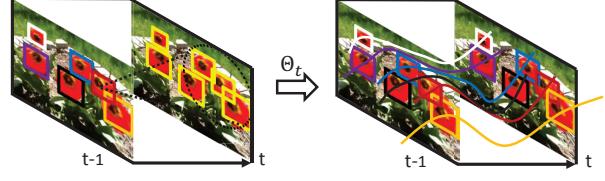

Figure 5: *Object labels are propagated from trajectories (different colors mean different objects) in frame $t-1$ to detection responses in frame t. Note the proximity of a flower indicated by the black dashed circle (best viewed in color).*

scribed above, we have

$$\mathcal{L}_C(\mathbf{W}_t) = \underbrace{\alpha \, tr(\mathbf{W}_t(\eta\mathbf{I}+\mathbf{M}_t)^{-1}\mathbf{W}_t^T)}_{regularization} +$$

$$\underbrace{\frac{\lambda}{2}\|\frac{1}{m}\sum_{i=1}^{m}\mathbf{X}_{u,t}^T\mathbf{w}_{t,i}-\mathbf{\Psi}(P_t)\|^2}_{spatio-temporal\ consistency} + \underbrace{\sum_{i=1}^{m}\frac{1}{2N_{t,i}}\|\mathbf{X}_{l,t,i}^T\mathbf{w}_{t,i}-\mathbf{Y}_{t,i}\|^2}_{loss}$$

$$s.t.\ tr(\mathbf{M}_t)=k, \mathbf{M}_t\preceq\mathbf{I}, \mathbf{M}_t\in\mathbf{S}_+^m$$

$$(5)$$

We treat this as a joint convex problem with regard to $\mathbf{W}$ and $\mathbf{M}$ [2]. Following [32], we adopt the Accelerated Project Gradient method to optimize this function. Labels of $\mathbf{X}_{u,t}$ are obtained by averaging the scores of all detectors as:

$$\mathbf{Y}_{u,t} = \frac{1}{m}\sum_{i=1}^{m}\mathbf{X}_{u,t}^T\mathbf{w}_{t,i} \quad (6)$$

We choose candidates with a score greater than zero and apply non-maximum suppression to output final class labels $\mathbf{Y}_{u,t}\in\{-1,1\}^N$.

3.3. Object label propagation

In the Bayesian formula Eq. 2, object label propagation is $P(Z_t|X_t,Y_t,Z_{0:t-1})$, where the estimation of Z_t is conditioned on detection responses Y_t and the history of estimations $Z_{0:t-1}$. Let the n trajectories at time $t-1$ be

$$T=\{T_i|T_i=<T_i^A,T_i^M,T_i^C>, i=1,...,n\}, \quad (7)$$

where T_i^A, T_i^M and T_i^C indicate appearance, motion, and context information, and let the m detection responses at time t be

$$D=\{D_j|D_j=<D_j^A,D_j^L,D_j^C>, j=1,...,m\}, \quad (8)$$

where D_j^A, D_j^L and D_j^C represent the appearance, location and context information. Tracking is carried out by propagating object labels from trajectories to detection responses via a configuration variable $\mathbf{\Theta}_t \in \mathbb{R}^{n\times m}$. Initially, all the elements of $\mathbf{\Theta}_t$ are 0. If an element $\mathbf{\Theta}_{tij}$ is switched to 1, then the label of trajectory T_i is propagated to detection response D_j, and the propagated quantity depends on the affinity $S(T_i \rightarrow D_j)$ between T_i and D_j (here "$\rightarrow$" means considering D_j as a component of T_i at time t), which is determined by appearance, motion and context. Fig. 5 shows this process. Objects are assumed to move smoothly, so we only consider detection responses within T_i's spatio-temporal proximity Ω_i (a circle with radius d_{Th}) and minimize the following energy function:

$$\mathcal{L}_O(\mathbf{\Theta}_t) = -\sum_i\sum_{j\in\Omega_i}S(T_i\rightarrow D_j)\mathbf{\Theta}_{tij}. \quad (9)$$

Appearance Model. We simply consider the intensity cue for appearance affinity. The appearance model T_i^A of trajectory T_i consists of the last 15 templates of this object, and the appearance similarity between D_j and T_i is

$$S_A(T_i\rightarrow D_j) = med(\text{NCC}(T_i^A,D_j^A)), \quad (10)$$

where $\text{NCC}(\bullet,\bullet)$ is the normalized cross-correlation (NCC) similarity measure and $med(\bullet)$ is the median.

Motion Model. We maintain the past three displacements and predict a displacement vec_i weighted by $[\frac{4}{7},\frac{2}{7},\frac{1}{7}]$, where older values are weighted higher. Given D_j, the actual displacement vec_j is the difference between D_j^L and the most recent location of the object corresponding to T_i. The motion affinity is

$$S_M(T_i\rightarrow D_j) = cos(vec_i,vec_j). \quad (11)$$

Context Model. In modeling context information, we follow the work in [22] and employ 2D histograms of
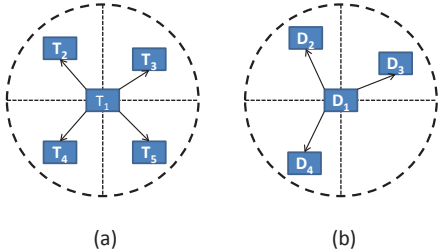
Figure 6: *Context model. Contexts of (a) trajectories and (b) detection responses are modeled by histograms, counting objects within an object's proximity.*

nearby objects to improve the robustness. As shown in Fig. 6, there are (a) five trajectories and (b) four detection responses. To compute a histogram for T_i, we divide the neighborhood of T_i into M partitions (here $M = 4$ for sake of display). For each object located in this neighborhood we compute a distance vector relative to T_i. According to the distance vector, we accumulate the distance values for each partition. By normalization, we obtain an M-bin histogram $\mathbf{H}_i$. The context affinity is

$$S_C(T_i \rightarrow D_j) = exp(-Bhatt(\mathbf{H}_i, \mathbf{H}_j)). \quad (12)$$

Having obtained affinities based on three cues, we combine them as follows:

$$S(T_i \rightarrow D_j) = S_A(T_i \rightarrow D_j) * S_M(T_i \rightarrow D_j) * S_C(T_i \rightarrow D_j). \quad (13)$$

We minimize the energy (Eq. 9) by greedy search in an iterative way. First we turn off all propagation switches. We then compute the affinities of all propagation pairs and turn on the propagation switch (say T_i and D_j) which most decreases the energy. At the same time, D_j is labeled as the extension of T_i. We remove this pair of trajectory and detection response from the search space. This procedure is repeated until there is no further energy decrease. Finally, trajectories outside the search space are updated considering the extended component. The remaining trajectories in the search space are terminated, and new trajectories are initialized based on detection responses in the search space. For clarity, the algorithm is summarized in Algorithm 1.

4. Experiments

4.1. Data sets & Setup

We test our algorithm on eight data sets, Airshow, Goose, Sailing, Zebra, Crab, Antelope, Flower[1] and Hockey. The first three are new sequences obtained from YouTube videos, and the last five are public sequences [18, 20, 31]. These data sets are challenging as they contain (1) crowd

---

[1]This sequence is part of the original sequence in [31] (500 frames of the original 2249 frames)

Algorithm 1: Object label propagation for MOT

Data: T, D, proximity set Ω.

Result: Θ_t, labels of detection responses.

1 **Initialization**: $\Theta_t = \mathbf{0}$.

2 **while** $\mathcal{L}_O$ *decrease,* **do**

3   **foreach** $T_i \in T$ *and* $D_j \in \Omega_i$, **do**

4   compute the energy decrease of T_i and D_j.

5   find T_i and D_j with the greatest decrease via Eq. 9

6   set $\Theta_{tij} = 1$, propagate the label of T_i to D_j.

7   remove T_i and D_j, update the proximity set Ω.

8 Terminate trajectories in T, initialize trajectories according to detection responses in D.

---

scenarios with similar objects, (2) partial or complete occlusions, (3) background clutter, and (4) out-of-plane rotations. Parameters λ, α and η in Eq. 5 are set to be 0.1, 0.001 and 0.001 respectively. The proximity parameter d_{Th} is 20. The number of detectors is 12. For each task, we sample $\frac{2}{3}$ instances from the whole training data. We extract HoG [9], LBP and colors as features for object detection. The threshold to determine the confident instances is 0.5. Note that for the public data sets, we refer to results reported in [18]. For data sets which are not public, we obtain results by running the authors' code ([13, 31]) or by re-implementing the method ([18] and **K-SVM**).

4.2. Generic object detection

We conducted experiments on generic object detection to verify the effectiveness of the proposed cMTL based detection method. Five methods were compared: (1) **TLD** [13] which uses a detector based on Random Ferns; (2) **K-SVM**. We train K independent SVMs on clustered training data from K-means clustering and detect objects by classification. This is a typical way to handle intra-class variance. The number of SVMs is four; we use the same number of clusters in our algorithm; (3) **GMOT** [18] is a framework which handles the same problem with a detector based on a Laplacian SVM; (4) our baseline method **BL** which uses cMTL without the spatio-temporal consistency; (5) our full method. Table 1 shows the results. A detection response is defined as true positive if its overlap with the ground truth bounding box is at least 0.5.

The results indicate that: (1) **TLD** only discovers a small portion of objects on some sequences. We suspect that this is due to limitations of the **TLD** detector which uses two-pixel comparisons and therefore cannot handle large intra-class variance; (2) **K-SVM** and **GMOT** show good performance, and **BL** generally outperforms these, showing the effectiveness of cMTL to handle intra-class variance; (3) the full method outperforms all other methods; in comparison with **BL** the recall rate is increased due to the spatio-

Table 1: *Generic object detection results in terms of recall and precision values. The best results are shown in bold, the second best are underlined.*

Sequence	Recall					Precision				
	TLD	GMOT	K-SVM	BL	Ours	TLD	GMOT	K-SVM	BL	Ours
Antelope	.29	.74	.88	.77	**.89**	.57	.66	.71	.76	**.77**
Goose	.66	.80	.92	.85	**.94**	.94	.85	.97	.98	**.99**
Zebra	.60	.80	.66	.74	**.82**	.92	**.97**	.88	.91	.91
Crab	.22	.52	.55	.56	**.58**	.58	.81	.70	.85	**.88**
Flower	.21	.47	.30	.50	**.63**	.58	.62	**.95**	.94	.91
Airshow	.16	.13	.38	.43	**.63**	.52	.56	.76	**.77**	.75
Sailing	.60	.63	.56	.67	**.84**	**1**	.93	**1**	**1**	.99
Hockey	.65	**.84**	.43	.65	.82	.92	.89	.75	.88	**.94**
Avg.	.56	.56	.56	.61	**.70**	.67	.79	.79	.88	**.89**

Table 2: *Comparative results for different values of K (number of SVMs in K-SVM and, correspondingly, number of clusters in our method).*

Sequence	Method	Recall					Precision				
	$K=$	2	4	6	8	*Avg.*	2	4	6	8	*Avg.*
Antelope	K-SVM	.90	.88	.86	.84	**.87**	.66	.71	.72	.73	.70
	Ours	.83	.89	.80	.80	.82	.81	.77	.81	.80	**.80**
Zebra	K-SVM	.66	.66	.70	.70	.68	.88	.88	.89	.87	**.88**
	Ours	.73	.82	.72	.72	**.75**	.85	.91	.84	.84	.86

Figure 7: *Precision-Recall performance of* **TLD** *and* **BL** *on the* Antelope *and* Zebra *sequences.*
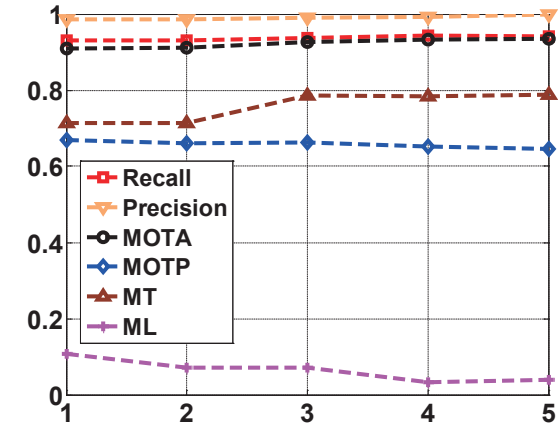
Figure 8: *Performance variation of five different initializations on the* Goose *sequence.*

temporal consistency.

In a separate experiment we vary the number K in **K-SVM** as well as the corresponding number of clusters in our algorithm. Two representative public sequences (Antilope and Zebra) are used in this experiment. Table 2 shows the results, which demonstrate that our algorithm outperforms **K-SVM** for most K in terms of recall rate, which is important in our setting. Note that we keep K fixed for the other experiments; a suitable choice of K is beyond the scope of this paper.

In a more extensive comparison of the baseline method with **TLD** we obtain the precision-recall curves for the Antelope and Zebra sequences, shown in Fig. 7. **BL** uses a threshold on the score value to determine whether a candidate is an object, and **TLD** [13] uses the percentage of ferns voting for a positive decision. The results show that our baseline method outperforms **TLD** consistently.

To test the variation of performance resulting from different initial bounding boxes, we run our algorithm five times on the Goose sequence, each time labelling a different initial object. The recall rates are 0.935 ± 0.006 and the precision rates 0.990 ± 0.004, indicating low dependence on the initialization (see Fig. 8).
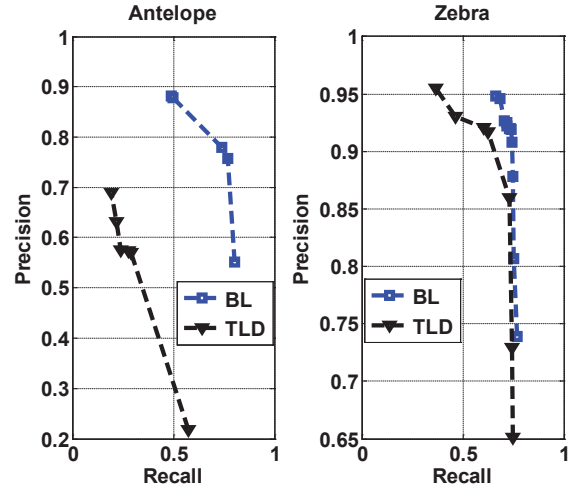
4.3. Generic MOT

We carried out experiments to compare our framework with several state-of-the-art methods on the task of detecting and tracking multiple objects. The experiments are presented in three parts:

(1) For each sequence we compare with **TLD** [13] and **GMOT** [18]. **TLD** was originally developed for single object tracking, and we extended it to multiple objects by decreasing the threshold to let it detect some similar objects and track them. It is initialized with the same bounding box as other methods.

(2) For the Zebra, Crab, Flower, Airshow and Sailing sequences, we apply **SPOT** [31] to track multiple objects (four in our experiments) in each sequence. To compare the performance, we excerpt results corresponding to these four objects from our whole result in each sequence and evaluate the results. It is worth noting that our algorithm starts with

a single bounding box while **SPOT** [31] starts with all four bounding boxes for each sequence.

(3) For the Hockey sequence, we additionally compare with [7, 6, 20] using the results from [18].

Example images are shown in Fig. 9. We adopt the criteria of Multiple Object Tracking Accuracy (MOTA), Multiple Object Tracking Precision (MOTP) proposed in [5] as well as Mostly Tracked (MT) trajectories and Mostly Loss (ML) trajectories [17] to give quantitative results. MOTA takes the missed detection, false positives and false matches into consideration. MOTP measures the average overlap between the ground truth and the true positive. MT is the ratio of the ground truth trajectories which are covered by tracking results for more than 80% in length. ML is the ratio of the ground truth trajectories which are covered by tracking results for less than 20% in length. As shown in Table 3, the arrows following the criteria indicate the trend of better performance.

Results in Table 3 show that: (1) compared with **TLD** and **GMOT**, our method outperforms other methods on most sequences; (2) compared with **SPOT**, our approach achieves better results except on the MOTP metric. We suspect that this is due to **SPOT** trackers being object-specific, thereby obtaining greater overlap scores, *i.e.* larger MOTP values; (3) for the Hockey sequence, our method obtains results comparable with methods that use a specific off-line trained human detector.

In order to test the sensitivity on different initializations, we run our algorithm on the Goose sequence five times with different initial bounding boxes. The MOTA, MOTP, MT and ML are 0.935 ± 0.012, 0.660 ± 0.009, 0.750 ± 0.042 and 0.071 ± 0.029 respectively (see Fig. 8), indicating low sensitivity to the initial labeling.

5. Conclusion

This paper proposed a framework for tracking multiple objects of the same general type, where class and object labels are propagated in the spatio-temporal domain. We introduced cMTL for generic object detection and have shown the benefit of including spatio-temporal consistency. The proposed method takes a sequential approach, entailing the limitation that object trajectories may be more fragmented than when taking a more global view of the data. Comparative experiments on eight sequences (five public and three new data sets) confirmed the effectiveness of the proposed method. From a practical viewpoint an advantage of our method over most other work in the area is the requirement of labeling just a single initial bounding box, thereby providing a multi-object tracker without resorting to an off-line trained detector.

Table 3: *Generic Multiple Object Tracking results. The table shows results in terms of four performance criteria from the literature (arrows indicating direction of better performance) on five public and three new datasets.*

Sequence	Method	MOTA ↑	MOTP↑	MT ↑	ML ↓
Antelope	TLD [13]	.088	.650	.235	.765
	GMOT [18]	.356	.633	.368	.368
	Our method	**.622**	**.714**	**.691**	**.177**
Goose	TLD[13]	.621	.611	.286	.179
	GMOT [18]	.798	.604	.643	.071
	Our method	**.938**	**.649**	**.786**	**.036**
Zebra	TLD [13]	.587	.645	.159	.420
	GMOT [18]	**.777**	.668	.435	.304
	Our method	.743	**.683**	**.580**	**.246**
	SPOT [31]	.661	**.753**	.750	0
	Our method	**.982**	.747	**1**	0
Crab	TLD [13]	.068	.646	.049	.864
	GMOT [18]	.391	.600	.097	.709
	Our method	**.497**	**.692**	**.214**	**.689**
	SPOT [31]	.190	**.766**	.500	.250
	Our method	**.924**	.724	**1**	**0**
Flower	TLD [13]	.053	.677	0	.632
	GMOT [18]	.186	.650	.053	.421
	Our method	**.566**	**.718**	**.316**	**.368**
	SPOT [31]	.372	.730	.500	.250
	Our method	**.524**	**.737**	.500	**0**
Airshow	TLD [13]	.013	.596	0	.733
	GMOT [18]	.028	**.716**	0	.867
	Our method	**.415**	.646	0	**.067**
	SPOT [31]	-.503	**.676**	0	.250
	Our method	**.346**	.650	0	**0**
Sailing	TLD [13]	.403	**.737**	.250	.083
	GMOT [18]	.548	.684	.250	.083
	Our method	**.819**	.640	**.833**	.083
	SPOT [31]	.554	**.731**	.750	.250
	Our method	**.786**	.652	.750	**0**
Hockey	TLD [13]	.547	.647	.179	.250
	GMOT [18]	**.803**	.691	**.679**	**.107**
	Our method	.766	**.736**	.607	.143
	Brendel *et al.* [7]	.797	.600	-	-
	Breitenstein *et al.* [6]	.765	.570	-	-
	Okuma *et al.* [20]	.678	.510	-	-
Avg.	TLD [13]	.279	.655	.140	.602
	GMOT [18]	.410	.637	.310	.427
	Our method	**.613**	**.685**	**.482**	**.336**
	SPOT [31]	.235	**.728**	.500	.200
	Our method	**.629**	.703	**.650**	**0**

References

[1] K. Ali, D. Hasler, and F. Fleuret. FlowBoost-appearance learning from sparsely annotated video. In *CVPR*, 2011.

[2] A. Argyriou, M. Pontil, Y. Ying, and C. A. Micchelli. A spectral regularization framework for multi-task structure learning. In *NIPS*, 2007.
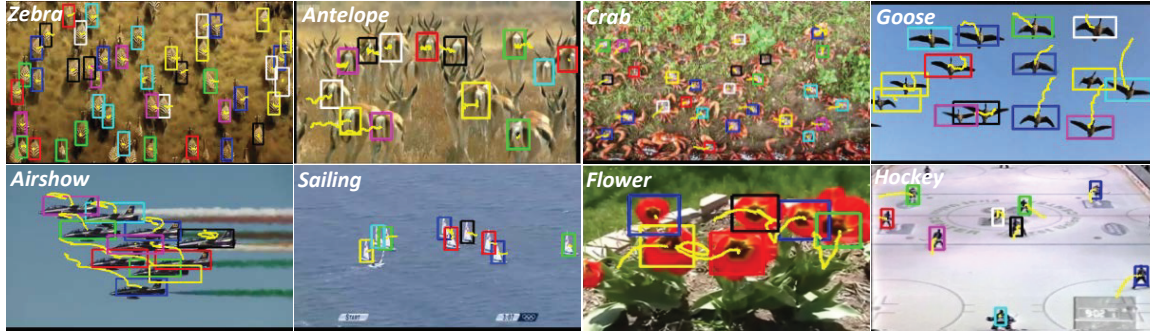
Figure 9: *Multiple object tracking results shown on frames excerpted from the videos. Different colors correspond to different objects (we only adopt 8 colors so some boxes are of the same color), the yellow lines represent trajectories.*

[3] V. Badrinarayanan, F. Galasso, and R. Cipolla. Label propagation in video sequences. In *CVPR*, 2010.

[4] J. Berclaz, F. Fleuret, E. Turetken, and P. Fua. Multiple object tracking using k-shortest paths optimization. *PAMI*, 33(9):1806–1819, 2011.

[5] K. Bernardin and R. Stiefelhagen. Evaluating multiple object tracking performance: the CLEAR MOT metrics. *EURASIP Journal on Image and Video Processing*, 2008.

[6] M. Breitenstein, F. Reichlin, B. Leibe, E. Koller-Meier, and L. Van Gool. Robust tracking-by-detection using a detector confidence particle filter. In *ICCV*, 2009.

[7] W. Brendel, M. Amer, and S. Todorovic. Multiobject tracking as maximum weight independent set. In *CVPR*, 2011.

[8] A. A. Butt and R. T. Collins. Multi-target tracking by lagrangian relaxation to min-cost network flow. In *CVPR*, 2013.

[9] N. Dalal and B. Triggs. Histograms of oriented gradients for human detection. In *CVPR*, 2005.

[10] T. Evgeniou and M. Pontil. Regularized multi–task learning. In *ACM SIGKDD*, 2004.

[11] P. Felzenszwalb, R. Girshick, D. McAllester, and D. Ramanan. Object detection with discriminatively trained part-based models. *PAMI*, 32(9):1627–1645, 2010.

[12] J. Henriques, R. Caseiro, and J. Batista. Globally optimal solution to multi-object tracking with merged measurements. In *ICCV*, 2011.

[13] Z. Kalal, K. Mikolajczyk, and J. Matas. Tracking-learning-detection. *PAMI*, 34(7):1409–1422, 2012.

[14] L. Kratz and K. Nishino. Tracking with local spatio-temporal motion patterns in extremely crowded scenes. In *CVPR*, 2010.

[15] C. Kuo, C. Huang, and R. Nevatia. Multi-target tracking by on-line learned discriminative appearance models. In *CVPR*, 2010.

[16] B. Leibe, K. Schindler, N. Cornelis, and L. Van Gool. Coupled object detection and tracking from static cameras and moving vehicles. *PAMI*, 30(10):1683–1698, 2008.

[17] Y. Li, C. Huang, and R. Nevatia. Learning to associate: HybridBoosted multi-target tracker for crowded scene. In *CVPR*, 2009.

[18] W. Luo and T.-K. Kim. Generic object crowd tracking by multi-task learning. In *BMVC*, 2013.

[19] A. Milan, K. Schindler, and S. Roth. Detection-and-trajectory-level exclusion in multiple object tracking. In *CVPR*, 2013.

[20] K. Okuma, A. Taleghani, N. de Freitas, J. Little, and D. Lowe. A boosted particle filter: Multitarget detection and tracking. In *ECCV*, 2004.

[21] S. Pellegrini, A. Ess, K. Schindler, and L. Van Gool. You'll never walk alone: Modeling social behavior for multi-target tracking. In *ICCV*, 2009.

[22] V. Reilly, H. Idrees, and M. Shah. Detection and tracking of large number of targets in wide area surveillance. In *ECCV*, 2010.

[23] X. Shi, H. Ling, X. J., and W. Hu. Multi-target tracking by rank-1 tensor approximation. In *CVPR*, 2013.

[24] G. Shu, A. Dehghan, O. Oreifej, E. Hand, and M. Shah. Part-based multiple-person tracking with partial occlusion handling. In *CVPR*, 2012.

[25] B. Song, T. Jeng, E. Staudt, and A. Roy-Chowdhury. A stochastic graph evolution framework for robust multi-target tracking. In *ECCV*, 2010.

[26] Z. Wu, A. Thangali, S. Sclaroff, and M. Betke. Coupling detection and data association for multiple object tracking. In *CVPR*, 2012.

[27] K. Yamaguchi, A. Berg, L. Ortiz, and T. Berg. Who are you with and where are you going? In *CVPR*, 2011.

[28] B. Yang and R. Nevatia. An online learned CRF model for multi-target tracking. In *CVPR*, 2012.

[29] M. Yang, F. Lv, W. Xu, and Y. Gong. Detection driven adaptive multi-cue integration for multiple human tracking. In *ICCV*, 2009.

[30] Y. Yang, G. Shu, and M. Shah. Semi-supervised learning of feature hierarchies for object detection in a video. In *CVPR*, 2013.

[31] L. Zhang and L. van der Maaten. Structure preserving object tracking. In *CVPR*, 2013.

[32] J. Zhou, J. Chen, and J. Ye. Clustered multi-task learning via alternating structure optimization. In *NIPS*, 2011.